Research Article / Review Article FUPRE JOURNAL 8(3): 01- 19(2024)

FUPRE Journal

of

Scientific and Industrial Research

ISSN: 2579-1184(Print) ISSN: 2578-1129 (Online)

http://fupre.edu.ng/journal

Slip and Induced Magnetic Field Effects on Tangential Hyperbolic Hybrid Nanofluid over a Stretching Wedge with Nonuniform Heat Source

OGUNNIYI, P.O. [1,*], ***OKEDOYE, A. M.*** [2]

[1,2] *Department of Mathematics, Federal University of Petroleum Resources Effurun, Delta State, Nigeria.*

ARTICLE INFO

Received: 11/12/2023
Accepted: 12/05/2024

Keywords

Heat-mass transfer, Magnetic Field, Nano-fluid, Non-Uniform Heat Source, Slip flow, Stretching Wedge.

ABSTRACT

Hybrid nanofluid flow analyses have obtained a lot of attention due to their usefulness as coolants in hybrid electric vehicles, health care, thermal exchange systems, cancer thermo-therapy, nuclear reactors, microfluidics, aerospace, acoustics, naval structures and power generation in power plants, This research investigated the impacts of slip and induced magnetic field effects on tangential hyperbolic hybrid nanofluid over a stretching wedge with non-uniform heat source. The nanoparticles used in this work are aluminum oxide (Al_2O_3) and copper (Cu) while water is the based fluid. The fluid flow are modelled as partial differential equations (PDEs). These are transformed to their corresponding ordinary forms (ODEs), which are solved by the homotopy analysis technique with the aid of similarity variables. The impact of prominent physical factors on fluid temperature, velocity, induced magnetic field, local Nusselt number and drag coefficient is explored. Tables and graphs are used to display the results which agreed with the existing ones in the literature.

1. INTRODUCTION

Amid the past few decades there has been a creating intrigued to see at the boundary layer fluid flows on a continuous extending sheet due to its great measured in designing and mechanical applications such as hot rolling, metallic turning, glass-fiber and paper generation, metal and polymer expulsion, wire drawing, and drawing of plastic movies. Crane 1970, investigated the boundary layer float activated through a directly extending sheet. Afterward, Carragher and Crane explored the research with warm radiation impact (Carragher and Crane, 1982). The normal boundary layer float on an exponentially extending continuous surface with an exponential temperature conveyance is explored by Magyari and Keller (1999). Partha et al., (2005), considered the impact of thick dissemination on the blended convection warm exchange from an exponentially extending surface. Bidin and Nazar, (2009) expanded this issue by examining the radiation impacts on the flow over an exponentially extending sheet and unraveled the bother of the sheet numerically. Ishak (2011), on numerically analyzed MHD boundary layer flow on an exponentially extending sheet in the presence of radiation through the utilization of Keller's strategy. Also, the influence of radiation on MHD flow

*Corresponding author, e-mail: *peteroolmi@yahoo.com*
DIO

over a stretching wedge was investigated (Ogunniyi et al., 2022).

The slip boundary situation is a well-understood phenomenon involving the non-adherence of fluids to surfaces. Fluids that demonstrate slip are beneficial in a range of fields, which include the cleaning of synthetic heart valves and indoors cavities. The Knudsen number, which is a measure of the molecular free path to characteristic length. When the Knudsen range is very tiny, no slide between the floor and the fluid is observed, which is in accordance with the essence of continuum mechanics. A slide glide boundary condition was once proposed by Beavers and Joseph (1967). Afify et al., (2014), quantitatively investigated the effects of thermal radiation, Newtonian heating, and the slip speed phenomenon on MHD flow and heat transmission across a permeable stretched sheet.

No-slip boundary circumstance (the presumption that a fluid follows to a strong boundary) is utilized to achieve the outcome of all the over expressed ponders. The no-slip boundary condition is one of the central suspicions of the Navier–Stokes hypothesis. Be that as it may, fractional speed slip (the non-adherence of the liquid to a solid boundary) may also happen on the extending boundary when the liquid is particulate such as emulsions, suspensions, froths and polymer arrangements. As of late, numerous analysts have examined the float issues taking slip drift condition at the boundary. Cleaning of engineered coronary heart valves and insides cavities are a few of vital innovative capacities of the liquids that grandstand boundary slip. Gbadeyan, Abubakar and Oyekunle, (2020), investigated impact of Navier slip on a steady incompressible fluid flow within a spiral channel by means of Adomian decomposition scheme. The result established that increased slip parameter increases the heat transfer at the wavy wall but reduces it at a flat wall. Aziz, Siddique and Aziz, (2014), numerically worked on a steady boundary layer slip flow through a permeable plate deep-seated in a penetrable medium. The outcome of the research demonstrated that porosity of the medium enhances the fluid velocity but opposes the thermal boundary layer of the fluid.

The extra magnetic field which is created on an electrically conducting fluid from an external magnetic field is known as the induced magnetic field (IMF). The influence of a higher magnetic Reynolds number causes this phenomena. It is used in MRI, geophysics, glass manufacture, and MHD generators, among other things. In combination with blood flow, it plays a critical function in heart disease treatment, blood pumps and a variety of other biomedical applications. IMF is investigated on an elongated plate with sources/sinks on static electrically conducting fluid by Kumari et al. (1990). Ali et al., (2011), revisited the IMF on MHD flow over an extending sheet.

Due to its basic capacities within the metallurgy, space innovation, different healing center medications, pharmaceutical building businesses, polymer generation and nourishment handling innovation, colossal inquiry as of late has been conducted on the heat with mass exchange on a versatile sheet. Besides, combined heat with mass exchange models including homogeneous-heterogeneous responses are critical in an assortment of designing forms, hence they are accepting a parcel of consideration these days. Thus, workable applications can be

recognized in a few frameworks, Okedoye, et al., (2022), like drying, temperature and dampness conveyance all through agrarian areas and natural product tree forests, and edit misfortune due to solidifying.

Thus, we expand the work of Mohamed and Ahmed (2018) to incorporate heat buoyancy and variable heat source. It is our conviction that the outcomes of this investigate will advance profound understanding into the impact of variable heat source and heat buoyancy on tangential hybrid nano-fluid over an extending wedge with slip. The outcome of this work with past related articles particularly was ascertained (Mohamed and Ahmed, 2018).

2. METHODOLOGY

2.1. Problem Formulation

Let's think about a situation where there is a smooth flow of liquid, which is not turbulent, and is being heated and moves over a wedge shape. The fluid is assumed to be a conductor of electricity, behaves like a regular fluid, and its properties are only affected by the magnetic field and temperature in terms of its density. The effects of how much something floats and its weight compared to its size are assumed to be very small in the momentum Boussinesq approximation. Additionally, the effects of an applied electric field, Joule heating, and the Hall Effect are not accounted for. Also, the magnetic field is assumed to affect the fluid flows. The x-axis goes in the same direction as the plate, and the y-axis is perpendicular to the plate. If the fluid's x-component of velocity is u, y-component of velocity is v, temperature is T, and induced magnetic as Bi, where (i=1,2), and with assumption of both the Boussinesq and boundary-layer approximations, then the equations that describe this problem can be written as (Mohamed and Ahmed, 2018; Alphonsa, et al., (2021):

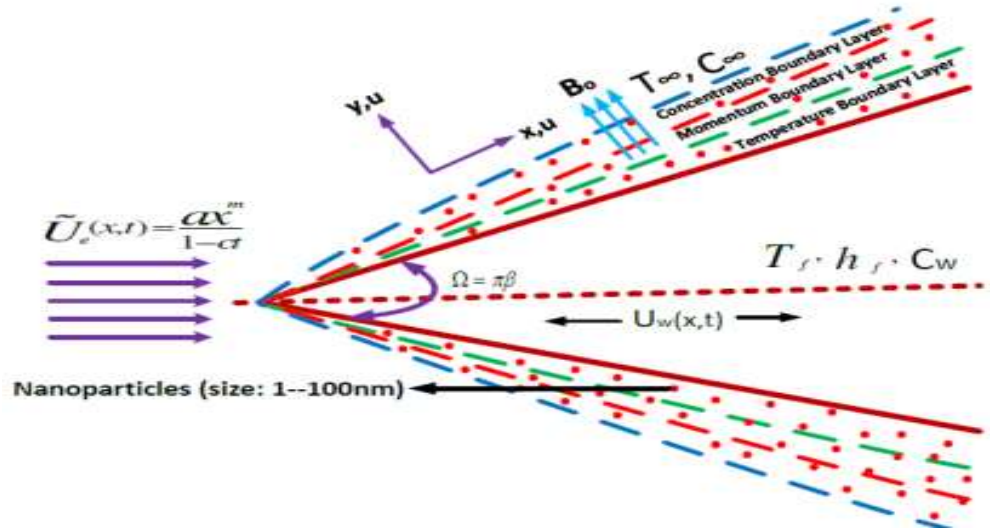

Figure 1: Schematic diagram for the flow (Ali et al., 2011)

$$\frac{\partial u}{\partial x}+\frac{\partial u}{\partial y}=0, \tag{1}$$

$$\frac{\partial B_1}{\partial x}+\frac{\partial B_2}{\partial y}=0, \tag{2}$$

$$u\frac{\partial u}{\partial x}+v\frac{\partial u}{\partial y}=u_e\frac{du_e}{dx}-\frac{\mu_{hnf}}{\rho_{hnf}}\left(\left(1+\frac{1}{\gamma}\right)+\sqrt{2}n\Gamma\left(\frac{\partial u}{\partial y}\right)\right)\frac{\partial^2 u}{\partial y^2}+\frac{\mu_e}{4\pi\rho_{hnf}}\left(B_1\frac{\partial B_1}{\partial x}+B_2\frac{\partial B_1}{\partial y}-B_e\frac{dB_e}{dx}\right) \tag{3}$$

$$u\frac{\partial B_1}{\partial x}+v\frac{\partial B_1}{\partial y}=B_1\frac{\partial u}{\partial x}+B_2\frac{\partial u}{\partial y}+\mu_0\frac{\partial^2 B_1}{\partial y^2}, \tag{4}$$

$$u\frac{\partial T}{\partial x}+v\frac{\partial T}{\partial y}=\frac{k_{hnf}}{\left(\rho c_p\right)_{hnf}}\frac{\partial^2 T}{\partial y^2}+\frac{q'''}{\left(\rho c_p\right)_{hnf}} \tag{5}$$

where μ_{hnf} is density of hybrid nanofluid, σ_{hnf} is electrical conductivity, q''' is rate of heat generation, k_{hnf} is the thermal conductivity of hybrid nanofluid, while $(\rho cp)_{hnf}$ represents the heat capacity of the hybrid nanofluid, η_0 is a measure of how magnetic fields spread out, μ_e is a measure of how easily magnetic fields pass through a material, $u_{w(x)}$ is the speed at which a sheet is being stretched, and $u_{e(x)}$ is the speed of the liquid flowing outside of the boundary layer. Constants c and a are positive numbers that determine the size of the stagnation point and how much the sheet is being stretched. L is the size of the stretching surface. $B_{e(x)}$ is the magnetic field at the boundary layer, which is estimated by B_0 (x/L). B_0 is the estimated uniform magnetic field at the beginning of the surface. Also, B1 and B2 are magnetic parts in the x and y directions, respectively.

The amount of heat produced is specified as

$$q'''=\frac{kU}{\nu x}\left(a\left(T_w-T_\infty\right)e^{-\eta}+b\left(T-T_\infty\right)\right)$$

$$q'''=\left(\frac{k_{hnf}u_w(x)}{x\nu_f}\right)\left[\frac{A^*(T_w-T_\infty)}{bx}u+Q_0(T-T_\infty)\right] \tag{6}$$

(Q_0, A^*) represents the temperature and space. The coefficient for the heat source or sink that depends on something. In addition, when A is greater than 0 and Q_0 is greater than 0, it means heat is being generated internally. On the other hand, when A is less than 0 and Q_0 is less than 0, it means heat is being absorbed internally.

So, equations (6) with equation (5) give:

$$\frac{\partial T}{\partial x} + v\frac{\partial T}{\partial y} = \frac{k_{hnf}}{(\rho c_p)_{hnf}}\frac{\partial^2 T}{\partial y^2} + \left(\frac{u_w(x)}{x\nu_f}\right)\left[\frac{A^*(T_w - T_\infty)}{cx}u + Q_0(T - T_\infty)\right] \quad (7)$$

The boundary conditions at the wedge surface and into the fluid are given as:

$$u = ax + U_{slip}\frac{\partial u}{\partial y}, v = 0, \frac{\partial B_1}{\partial y} = B_2 = 0, -\kappa_{hnf}\frac{\partial T}{\partial y} = h(T_f - T) \text{ at } y = 0$$
$$u \to U_0, B_1 \to B_0, T \to T_\infty \text{ as } y \to \infty \quad (8)$$

where h is the plate heat transfer coefficient, U_{slip} is the velocity slip factor, T_∞ is the free stream temperature, T_w is the hot fluid's temperature on the left side of the wedge and is called the wedge's temperature. The coefficient that measures how well heat can travel through the wedge is called the thermal conductivity coefficient.

2.2 Speed of Heat and Mass Movement at the wall

Two important parameters which have applications in engineering are discussed. These are the skin friction coefficient and the local Nusselt number. These measurements describe how easily something resists movement through a fluid and how much heat is transferred to a wall.

The quantities Skin friction coefficient and Nusselt number are denoted by c_f and Nu respectively and are defined similar to Mohamed and Ahmed 2018, as follows:

$$c_f = \frac{\tau_w}{\rho_{hnf}U_w^2}, \quad (9)$$

$$Nu = \frac{xq_w}{k_{hnf}(T_w - T_\infty)}, \quad (10)$$

where τ_w represents the skin friction along the surface, q_w the heat flux from the surface and are respectively given as

$$\tau_w = \left[\left(\mu_B + \frac{P_y}{\sqrt{2\pi_c}}\right)\frac{\partial u}{\partial y}\right]_{y=0}, \quad q_w = \left[-k_{hnf}\frac{\partial T}{\partial y}\right]_{y=0} \quad (11)$$

where U_w and q_w, represent the wall shear stress and heat transfer respectively.

2.3. Thermophysical Features

In the Table 1, presents the thermo-physical properties of Cu, water with Al_2O_3 according to (Mabood et al. 2020; Waini et al., 2020). Hybrid nanofluid's thermo-physical properties can be obtained from model in Table 2. The ϕ_1 and ϕ_2 denote the volume fractions of Al_2O_3 and Cu respectively, k is thermal conductivity, μ is the dynamic viscosity, σ is electrical conductivity, the density is represented by ρ, (ρcp) is the heat capacity, Cp is for constant pressure specific heat, where applicable the subscripts s_1, s_2 and f represent solid component for Al_2O_3, Cu nanoparticles and water respectively, whilst the subscripts *hnf* denoted hybrid nanofluid respectively.

*Corresponding author, e-mail: peteroolmi@yahoo.com
DIO

Table 1: The properties of water and the nanoparticles (Mabood et al., 2020; Waini et al., 2020)

Physical-properties	Al_2O_3	Cu	H_2O
$C_p \ \backslash JKg^{-1}K^{-1}$	765	385	4179
$\rho \ \backslash Kgm^{-3}$	3970	8933	997.1
$\kappa \ \backslash Wm^{-1}K^{-1}$	40	4×10^{2}	613×10^{-3}
$\sigma \ \backslash \mathrm{S}m^{-1}$	369×10^{5}	596×10^{5}	5×10^{-2}

Table 2: Thermophysical models of hybrid nanofluid (Mabood et al. 2020; Waini et al., 2020:

Properties	Hybrid Nanofluid (Al_2O_3 - Cu / H_2O)
Density	$\rho_{hnf} = \frac{\phi_2\rho_{s_2}}{\rho_f} - (\phi_2 - 1)\left[(1-\phi_1) + \frac{\rho_{s_1}\phi_1}{\rho_f}\right]$
Heat capacity	$(\rho C_p)_{hnf} = \left(\frac{(\rho C_p)_{s_2}\phi_2}{(\rho C_p)_f} - (\phi_2 - 1)\left[(1-\phi_1) + \frac{(\rho C_p)_{s_1}\phi_1}{(\rho C_p)_f}\right]\right)(\rho C_p)_f$
Viscosity	$\mu_{hnf} = \mu_f\left[(1-\phi_1)(1-\phi_2)\right]^{-2.5}$
Thermal conductivity	$\kappa_{hnf} = \frac{\kappa_{s_2} + 2(\kappa_{s_2} - \kappa_f)\phi_2 + 2\kappa_f}{\kappa_{s_2} + (\kappa_f - \kappa_{s_2})\phi_2 + 2\kappa_f} \times \frac{\kappa_{s_1} + 2(\kappa_{s_1} - \kappa_f)\phi_2 + 2\kappa_f}{\kappa_{s_1} + \phi_1(\kappa_f - \kappa_{s_1}) + 2\kappa_f}\kappa_f$
Electrical conductivity	$\frac{\sigma_{hnf}}{\sigma_f} = \left[1 + \frac{3(\sigma_{s_1}\phi_{s_1} - \phi\sigma_f) + \sigma_{s_2}\phi_{s_2}}{\sigma_{s_1}(1-\phi_{s_1}) + \sigma_{s_2}(1-\phi_{s_2}) + (2+\phi)\sigma_f}\right]$
	$\phi = \phi_1 + \phi_2$

2.4. Method of Solution

The stream function ψ used for velocity and magnetic field satisfied the continuity equation automatically. $u = \frac{\partial\psi_u}{\partial y}$ and $v = -\frac{\partial\psi_u}{\partial x}$, $u = \frac{\partial\psi_B}{\partial y}$ and $v = -\frac{\partial\psi_B}{\partial x}$ (12)

With similarity solution for equations (1) - (4) and (9), and a new variable η, the following in terms of the stream function ψ were defined as:

$$\eta = y\sqrt{\frac{U_w}{\nu_f x}}, \psi_u = \sqrt{\nu_f x U_w} f(\eta), \qquad \psi_B = \sqrt{\nu_f x B_e} g(\eta) \tag{13}$$

The dimensionless temperature is given as

$$\theta(\eta) = \frac{T - T_\infty}{T_w - T_\infty}. \tag{14}$$

But U_w and B_e are defined respectively as

$$u_w(x) = cx \text{ and } B_e(x) = B_0\left(\frac{x}{L}\right) \tag{15}$$

Equations (13) and (15) implies

$$\eta = y\sqrt{\frac{c}{\nu_f}}, \qquad \psi_u = x\sqrt{\nu_f c}f(\eta), \qquad \psi_B = x\sqrt{\frac{\nu_f B_0}{L}}g(\eta) \tag{16}$$

Hence, we can obtain the following identities from equations (12) and (16);

$$u = cxf'(\eta), v = -\sqrt{\nu_f c}f(\eta), B_1 = x\sqrt{\frac{cB_0}{L}}g'(\eta) \text{ and } B_2 = -\sqrt{\frac{\nu_f B_0}{L}}g(\eta) \tag{17}$$

Using equations (14) - (17), dimensionless form of (3), (4) and (9) are obtained as

$$A^2 + \frac{N_4}{N_1}\left((1-n) - nW_e\left(\frac{\partial^2 f(\eta)}{\partial\eta^2}\right)\right)\frac{\partial^3 f(\eta)}{\partial\eta^3} - \left(\frac{\partial f(\eta)}{\partial\eta}\right)^2 + f(\eta)\frac{\partial^2 f(\eta)}{\partial\eta^2} + \frac{1}{\mathrm{N}_1}H\left(\left(\frac{\partial g(\eta)}{\partial\eta}\right)^2 - g(\eta)\frac{\partial^2 g(\eta)}{\partial\eta^2} - 1\right) = 0 \tag{18}$$

$$\frac{\partial^3 g(\eta)}{\partial\eta^3} + \lambda\left(f(\eta)\frac{\partial^2 g(\eta)}{\partial\eta^2} - g(\eta)\frac{\partial^2 f(\eta)}{\partial\eta^2}\right) = 0 \tag{19}$$

$$\frac{N_3}{Pr}\frac{\partial^2\theta(\eta)}{\partial\eta^2} + \mathrm{N}_2 f(\eta)\frac{\partial\theta(\eta)}{\partial\eta} + \frac{1}{Pr}\left(\alpha\frac{\partial f(\eta)}{\partial\eta} + \beta\theta(\eta)\right) = 0 \tag{20}$$

Dimensionless form of boundary conditions (8) becomes

$$f'(0) = 1 + \lambda_1\frac{\partial^2 f(0)}{\partial\eta^2}, f(0) = S, \frac{\partial f(0)}{\partial\eta} = 1, g''(\eta) = 0, g(\eta) = 0, \frac{\partial\theta(0)}{\partial y} = -\omega(1-\theta(0))$$
$$\frac{\partial f(\eta)}{\partial\eta} \to A, \frac{\partial g(\eta)}{\partial\eta} \to 1, \theta(\eta) \to 0 \quad \text{as } \eta \to \infty \tag{21}$$

The emerging dimensionless flow governing parameters are defined by

$$W_e = \frac{\sqrt{2}\Gamma c^{\frac{3}{2}}x}{\sqrt{\nu_f}},\ Pr = \frac{\mu_f}{\rho_f c K_1},\ \lambda_1 = N\sqrt{\frac{c}{\nu_f}},\ \omega = \frac{h}{N3\kappa_f},\ H = \frac{u_e}{4\pi\rho_f}\frac{c^3x^2B_0}{L}$$
$$\lambda = \frac{\mu_0}{\nu_f}\ A = \frac{a}{c},\ N1 = \frac{\rho_{hnf}}{\rho_f}, N2 = \frac{(\rho c_p)_{hnf}}{(\rho c_p)_f},\ N3 = \frac{\kappa_{hnf}}{\kappa_f},\ N4 = \frac{\mu_{hnf}}{\mu_f}$$

2.4.1. Skin-Friction and wall Heat Transfer

Skin-friction refers to the resistance experienced by an object moving through a fluid due to the friction between the object's surface and the fluid. Wall heat transfer, on the other hand, involves the transfer of heat between a solid surface (such as a wall) and the fluid it is in contact with.

Engineering measurements of interest include the amount of friction experienced on the surface (local skin friction Cf_x) and the rate of heat transfer observed at a certain location (local Nusselt number Nu_x). In simple terms, we calculate the rate of heat transfer at the wall using Fourier's law, which tells us how the friction affects the surface and the Nusselt number shows how heat is transferred at the wall.

These measurements describe how heat and mass move on the wall's surface. They are defined as follows:

$$c_f = \frac{\tau_w}{\rho_{hnf}U_w^2} = \frac{\mu_{hnf}}{\rho_{hnf}U_w^2}\left[\left(\left(1+\frac{1}{\gamma}\right)+\sqrt{2n\Gamma}\right)\frac{\partial u}{\partial y}\right]_{y=0} = \frac{1}{\sqrt{Re}}\left[\left((1-n)-nW_e\right)\frac{\partial f'(\eta)}{\partial \eta}\right]_{y=0}$$

$$\Longrightarrow c_f(Re_x)^{1/2} = \left[\left((1-n)-nW_e\right)\frac{\partial f'(\eta)}{\partial \eta}\right]_{y=0}$$

$$Nu = \frac{xq_w}{k_{hnf}(T_w - T_\infty)} = -\sqrt{Re}\left[\frac{\partial \theta(\eta)}{\partial \eta}\right]_{y=0} \Longrightarrow Nu(Re_x)^{-1/2} = -\left[\frac{\partial \theta(\eta)}{\partial \eta}\right]_{\eta=0} \quad (22)$$

Where the local Reynolds number (Re_x) is define as $Re_x = xu_w/\nu_f$

2.4.2. Numerical Computation

The Homotopy analysis method (HAM) is a way to solve problems using base functions. We choose the base functions as defined in equation (23) because as we move towards infinity, the flows at the boundary layer decrease rapidly, Liao (1992; 2002).

The rule of solution for the base functions must be observed. Using the boundary conditions, we carefully select the initial approximations as:

$$f(\eta) = a_{0,0} + \sum_{k=0}^{\infty}\sum_{n=0}^{\infty} a_{k,n}\eta^k e^{-n\eta},\ g(\eta) = \sum_{k=0}^{\infty}\sum_{n=0}^{\infty} b_{k,n}\eta^k e^{-n\eta},\ \theta(\eta) = \sum_{k=0}^{\infty}\sum_{n=0}^{\infty} c_{k,n}\eta^k e^{-n\eta} \quad (23)$$

$$f(\eta) = 1 + \frac{1}{A+U_{slip}}\left(1-e^{-\eta}\right),\ g(\eta) = e^{-\eta},\ \theta(\eta) = \frac{\beta_i}{N_3}\left(e^{-\eta}-1\right) \quad (24)$$

Subsequently, which signify the auxiliary linear operators are chosen as:

$$L_f(f) = f'''(\eta) - f'(\eta),\ L_g(f) = g''(\eta) - g(\eta),\ L_\theta(f) = \theta''(\eta) - \theta(\eta) \quad (25)$$

The above equation (3) satisfies the following

$$L_f(c_1 + c_2 + c_3e^{\eta} + c_4e^{-\eta}) = 0,\ L_g(c_5 + c_6e^{\eta} + c_7e^{-\eta}) = 0,\ L_\theta(c_8e^{\eta} + c_9e^{-\eta}) = 0 \quad (26)$$

Zeroth-order deformation problem

*Corresponding author, e-mail: peteroolmi@yahoo.com
DIO

$$(1-p)L_f\left[f(\eta;p)-f_0(\eta)\right]=p\hbar N_f\left[f,g,\theta\right],\ (1-p)L_g\left[g(\eta;p)-g_0(\eta)\right]=p\hbar N_g\left[f,g,\theta\right]$$

$$(1-p)L_\theta\left[\theta(\eta;p)-\theta_0(\eta)\right]=p\hbar N_\theta\left[f,g,\theta\right] \tag{27}$$

In the equation (5), the embedding parameter is represented by the quantity, and the auxiliary parameter is $\hbar$.

$$N_f\left[f,g,\theta\right]=A^3+\frac{N_4}{N_1}(1-n)\frac{\partial^3}{\partial\eta^3}f(\eta;p)+\frac{N_4}{N_1}W\frac{\partial^3}{\partial\eta^3}f(\eta;p)-\left(f(\eta;p)\right)^2$$
$$+B^2\left(\frac{\partial}{\partial\eta}f(\eta;p)^2-f(\eta;p)\frac{\partial^2}{\partial\eta^2}g(\eta;p)+1\right)$$

$$N_g\left[f,g,\theta\right]=\frac{\partial^3}{\partial\eta^3}g(\eta;p)-\lambda_1\left(g\frac{\partial^2}{\partial\eta^2}f(\eta;p)-f\frac{\partial^2}{\partial\eta^2}g(\eta;p)\right)$$

$$N_\theta\left[f,g,\theta\right]=N_2 f\frac{\partial}{\partial\eta}\theta(\eta;p)+\frac{N_3}{\Pr}\frac{\partial^2}{\partial\eta^2}\theta(\eta;p)+\frac{1}{\Pr}\left(ae^{-\eta}+b\theta(\eta;p)\right) \tag{28}$$

The equation (6) is subject to the boundary conditions given by (7) below

$$f'(0,p)=1;\quad f'(0,p)=A+U_{slip}f''(0,p);\quad f(0,p)=0;\ f'(\infty,p)=0$$

$$g''(0,p)=0;\quad g(0,p)=0;\ g'(\infty,p)=1,\ \theta'(0,p)=\frac{\beta_i}{N_3}\left(\theta(0,p)-1\right);\quad \theta(\infty,p)=0 \tag{29}$$

2.4.3. Mth-Order Deformation Problems

If equation (5) is differentiated m-times with respect to p, multiplying the result with inverse of m! and subjecting p=0 we obtain the following which are higher-order deformation problem, given by (8) below

$$L_f\left[f_m(\eta)-\chi_m f_{m-1}(\eta)\right]=\hbar_f R_m^f(\eta),\ L_g\left[g_m(\eta)-\chi_m g_{m-1}(\eta)\right]=\hbar_g R_m^g(\eta)$$

$$L_\theta\left[\theta_m(\eta)-\chi_m\theta_{m-1}(\eta)\right]=\hbar_\theta R_m^\theta(\eta) \tag{30}$$

With the corresponding boundary conditions (9)

$$f_m'(0)=0;\quad f_m'(0)=U_{slip}f_m''(0);\quad f_m(0)=0;\ f_m'(\infty)=0$$

$$g_m''(0)=0;\quad g_m(0)=0;\ g_m'(\infty)=1,\ \theta_m'(0)=\frac{\beta_i}{N_3}\theta_m(0)=0;\ \theta_m(\infty)=0 \tag{31}$$

Where

$$f_m(\eta)=\frac{1}{m!}\frac{\partial^m f(\eta,p)}{\partial\eta^m},\qquad g_m(\eta)=\frac{1}{m!}\frac{\partial^m g(\eta,p)}{\partial\eta^m},\qquad \theta_m(\eta)=\frac{1}{m!}\frac{\partial^m \theta(\eta,p)}{\partial\eta^m}$$

$$R_m^f(\eta)=A^2+\frac{N_4}{N_1}(1-n)f_{m-1}^{'''}+\frac{N_4}{N_1}Wf_{m-1}^{'''}+B^2\left(\sum_{n=0}^{m-1}g_{m-1-n}^{'}g_n^{'}-\sum_{n=0}^{m-1}g_{m-1-n}^{'}g_n^{''}+1\right)+\sum_{n=0}^{m-1}f_{m-1-n}^{'}f_n^{''}-\sum_{n=0}^{m-1}f_{m-1-n}^{'}f_n^{'}$$

$$R_m^g(\eta)=g_{m-1}^{'''}-\lambda_1\left(\sum_{n=0}^{m-1}g_{m-1-n}f_n^{''}-\sum_{n=0}^{m-1}f_{m-1-n}g_n^{''}\right)$$

$$R_m^\theta(\eta)=N_2\sum_{n=0}^{m-1}f_{m-1-n}\theta_n^{'}+\frac{N_3}{\Pr}\theta_{m-1}^{''}+\frac{1}{\Pr}\left(ae^{-\eta}+b\theta_{m-1}\right) \tag{32}$$

And $\chi_m=\begin{cases}1, & m\geq 1\\ 0, & m\leq 1\end{cases}$

When p=0 and p=1, we have:

$$f(\eta,0)=f_0(\eta),\qquad f(\eta,1)=f(\eta)$$

$$g(\eta,0)=g_0(\eta),\qquad \mathrm{g}(\eta,1)=g(\eta)$$

$$\theta(\eta,0)=\theta_0(\eta),\qquad \theta(\eta,1)=\theta(\eta) \tag{33}$$

When p changes from initial value 0 to final value1. The $f(\eta,p), g(\eta,p), \theta(\eta,p)$ also vary from initial solutions $f_0(\eta), g_0(\eta), \theta_0(\eta)$ to final solutions $f(\eta), \mathrm{g}(\eta), \theta(\eta)$ respectively.

Employing Taylor's series approach, we get

$$f(\eta,p)=f_0(\eta)+\sum_{m=1}^{\infty}f_m(\eta)p^m\qquad f_m(\eta)=\frac{1}{m!}\frac{\partial^m}{\partial\eta^m}f(\eta,p)\Big|_{p=0}$$

$$g(\eta,p)=g_0(\eta)+\sum_{m=1}^{\infty}g_m(\eta)p^m\qquad g_m(\eta)=\frac{1}{m!}\frac{\partial^m}{\partial\eta^m}g(\eta,p)\Big|_{p=0}$$

$$\theta(\eta,p)=\theta_0(\eta)+\sum_{m=1}^{\infty}\theta_m(\eta)p^m\qquad \theta_m(\eta)=\frac{1}{m!}\frac{\partial^m}{\partial\eta^m}\theta(\eta,p)\Big|_{p=0} \tag{34}$$

The series in (12) convergent at $p=1$with appropriate value of the auxiliary parameter

The general solutions to the non-homogeneous equations are given below as

$$f_m(\eta)=f_m^*(\eta)+c_1^m+c_2^m+c_3^me^{\eta}+c_4^me^{-\eta}$$

$$g_m(\eta)=g_m^*(\eta)+c_5^m+c_6^me^{\eta}+c_7^me^{-\eta},\ \theta_m(\eta)=\theta_m^*(\eta)+c_8^me^{\eta}+c_9^me^{-\eta} \tag{35}$$

Where the scalars $C_i^m;\ i=1,2,\cdots,9$ with the conditions (9) at the boundary. These are given as

$$\theta_m(\eta)=\theta_m^*(\eta)+c_8^m e^{\eta}+c_9^m e^{-\eta},\ c_3^m=c_5^m=c_6^m=c_8^m=0,\ c_1^m=-c_2^m-f_m^*(0)$$

$$c_4^m=1+\frac{1}{A+U_{slip}}\left[f_m^{*'}(0)-U_{slip}f_m^{*''}(0)\right],\ c_7^m=g_m^*(0),\ c_9^m=\frac{\beta_i}{N_3}\left(\theta_m^*(0)-\theta^*(0)\right) \quad (36)$$

Conclusively, the resulting solutions are coded into a MATHEMATICA software which executed it on an Intel core i5 6G RAM computer.

3. DISCUSSION OF RESULT

3.1. Accuracy of Results

To make sure the method is correct, the results obtained were compared for f"(0) at different values of the stretching parameter A with the results from Mahapatra and Gupta 2002, and Ishak et al. 2006. In the absence of the magnetic field and when certain variables are equal to zero (β, Gr, ω, α), a study by Mohamed and Ahmed 2018, also explored this. The results of the comparison in Table 1 match very well, and the same is true for other Prandtl (Pr) numbers. In contrast to the previous solution provided, a Prandtl number that corresponds to plasma ($\Pr=0.71$) was used.

Table 3: Drag coefficient $Cf_x\ Re_x^{1/2}$ for different *A* values when $H=W=n=\ \alpha=Bi=\phi=0$

	Mahapatra and Gupta [21]	Ishak et al. [22]	Mohamed and Ahmed [15]	Current Study
0.1	-0.9694	-0.9694	-0.969386	-0.96938615
0.2	-0.9181	-0.9181	-0.918107	-0.91810709
0.5	-0.6673	-0.6673	-0.667263	-0.66726367
2.0	2.0175	2.0175	2.017500	2.01750280
3.0	4.7293	4.7294	4.729280	4.72928236

3.2. Result Discussion

Influences of fluid controlling parameters on heat with mass transfer of hybrid nanofluid such as thermal radiation, slippage, induced magnetic field, etc., over a stretching wedge is analyzed in this work. Homotopy analysis solutions for the temperature, velocity, and induced magnetic field profiles are obtained and validated Nusselt number and drag coefficient solutions. The results are presented in Figures 2 – 14. In the absence of radiation effect magnetic field with heat source/sink with constant thermal conductivity the present result reduced to those obtained by Hayat et al., 2015; Hayat et al., 2016 and Alphonsa et al. 2021.

3.2.1. Effects of Parameters Variation on Velocity Field

Figure 2 shows the positive effect of the stretching parameter (A) on fluid velocity, $f(\eta)'$. Increasing the parameter expands the velocity profile $f(\eta)'$of the fluid. It can be deduced from the graph that when A is equal to 1, the velocity patterns for both the nanofluid and hybrid nanofluid flows are the

same. Furthermore, it is noticed that when the velocity is 1, its rate becomes zero. Here, it implies that, the surface and the fluid are moving at the same speed and direction. It has also been noticed that when the stretching parameter A is greater than 1, the velocity profiles increase. However, the profile decreases when the values of A are less than 1. Figure 3 demonstrates how the magnetic parameter (H) affects the fluid velocity $f(\eta)'$. Increasing the parameter enhances the $f(\eta)'$. Figure 4 shows the Weissenberg number's (W) influence which measures the speed at which a material relaxes compared to the time it takes for a process to occur. When the parameter increases the velocity of the fluid decreases, and it makes the hydrodynamic boundary layer weaker.

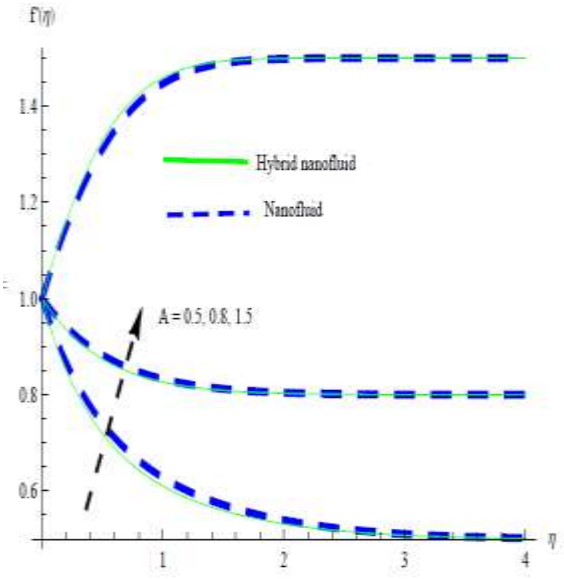

Figure 2: Effect of wedge's stretching parameter on fluid's velocity

3.2.2. Effects of Parameters Variation on Induced Magnetic Field

Figure 5 exhibits the negative impact of the stretching parameter (A) on the induced magnetic field. It is found from the figure that the induced magnetic field profile reduces with an increase in the stretching parameter for both cases of nanofluid and hybrid nanofluid. Figure 6 illustrates the positive impact of magnetic field parameter, H, on the induced magnetic field - $g(\eta)'$. Figure 7 shows that increasing W reduces the induced magnetic field profile. It shows that as the values of W increases, the induced magnetic field $g(\eta)'$decelerates. Figure 8 shows the mixed effect of the λ (reciprocal of magnetic Prandtl number) has different effects on $g(\eta)'$. At first, increasing λ values worsen the $g(\eta)'$, but later on, the reverse process occurred.

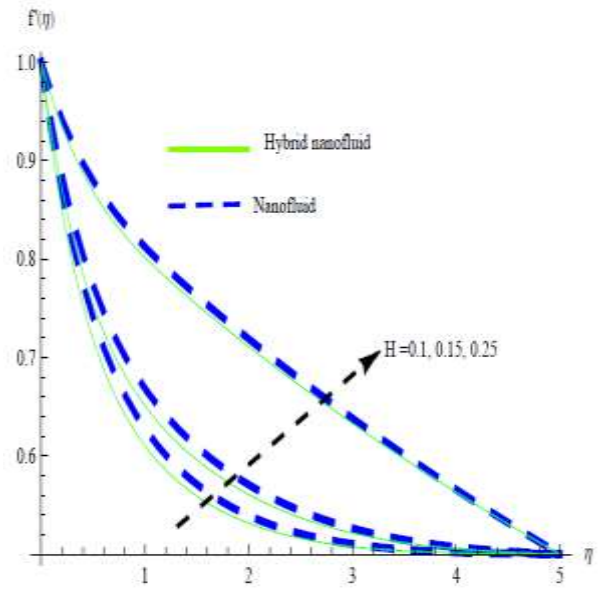

Figure 3: Impact of magnetic field on velocity profile

Table 4: The Rate of heat transfer at the wall of the stretching wedge

A	H	Λ	Rd	Ω	α	β	f''(0)	θ'(0)
0.5	*0.1*	*0.0*	*1.0*	0.1	0.2	-0.5	-0.668181	-1.314010
0.8							-0.321165	-1.341102
1.2							0.370392	-1.384380
	0.10						-0.668181	-1.314010
	0.15						-0.611117	-1.318683
	0.20						-0.531026	-1.325067
		0.1					-0.712080	-1.310420
		0.2					-0.693385	-1.311988
		0.25					-0.682010	-1.312916
			1.0				-0.682010	−1.312916
			3.0				-0.682010	−1.013755
			5.0				-0.682010	−0.861492
				0.3			-0.682010	−1.013755
				0.5			-0.682010	−0.861492
				0.7			-0.682010	−0.763582
					0.2		-0.682010	−1.312916
					0.4		-0.682010	−1.013755
					0.6		-0.682010	−0.861492
						-0.5	-0.682010	−1.341291
						0.5	-0.682010	−1.010750
						1.0	-0.682010	−0.844394

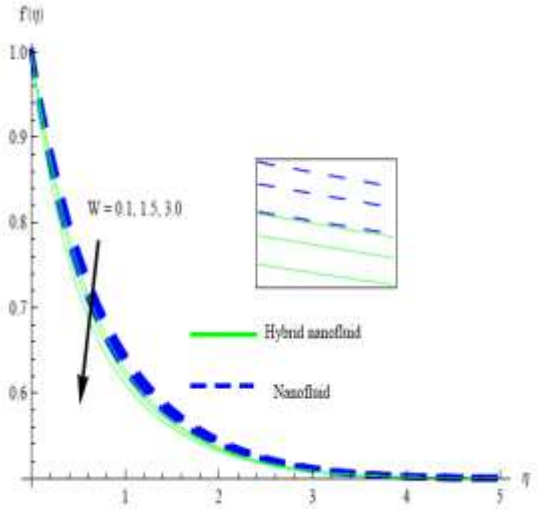

Figure 4: Influence of Weissenberg number on velocity profile

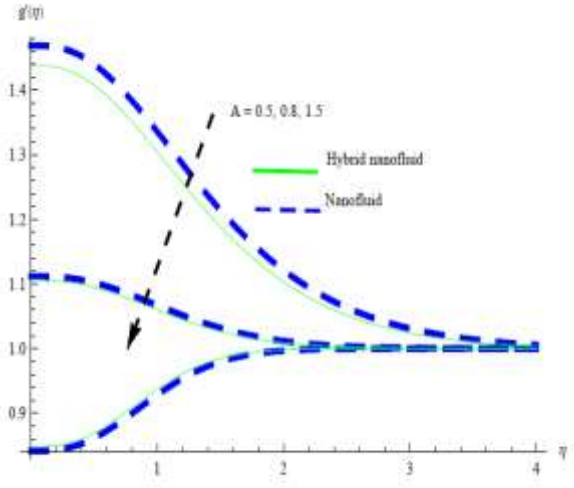

Figure 5: Variation of wedge's stretching parameter of fluid's induced magnetic field

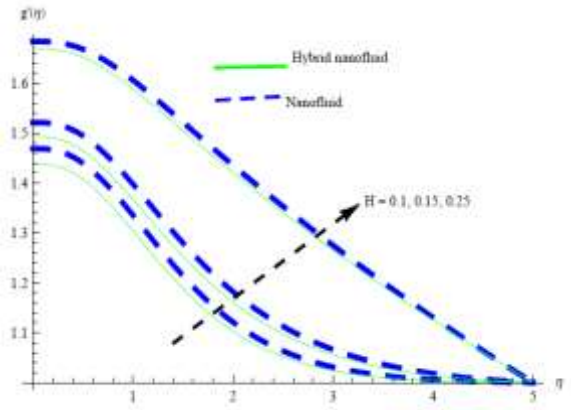

Figure 6: Impact of magnetic field on induced magnetic field profile

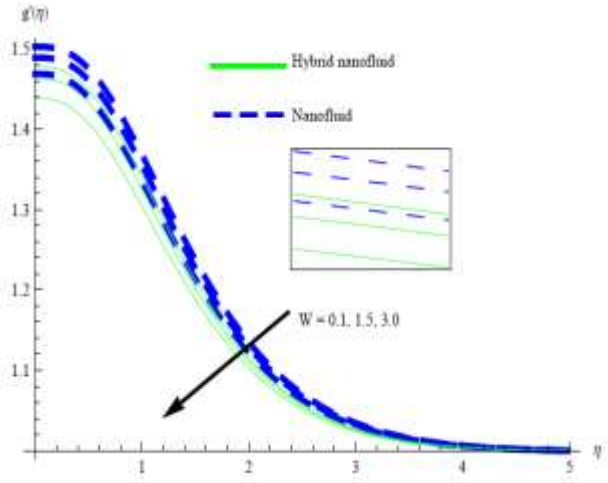

Figure 7: Influence of Weissenberg number on profile of induced magnetic field

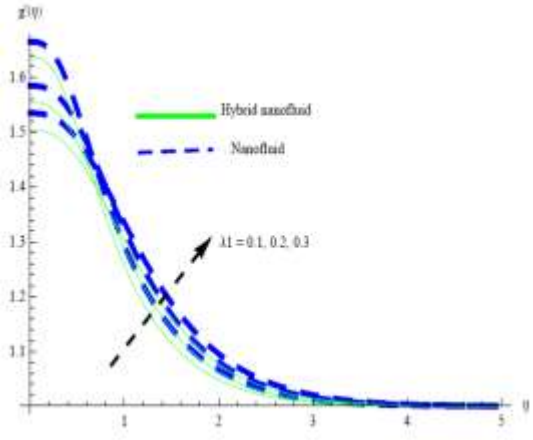

Figure 8: variation of reciprocal of induced brand tl number on induced magnetic field

*Corresponding author, e-mail: peteroolmi@yahoo.com
DIO

3.2.3. Effects of Parameters Variation on Temperature Field

The consequence of the stretching parameter, A, on fluid temperature is graphed in Figure 9, the temperature gets cooler as the parameter increases. It is important to mention that the temperatures are colder when using nanofluid with a higher stretching parameter compared to using hybrid nanofluid. Figure 10 demonstrates how the magnetic field parameter, H, affects the temperature field in both nanofluid and hybrid nanofluid flows. It lowers the temperature of the fluid on the system which enhances their performance and longevity. Figure 11 displays how the Weissenberg number influences the temperature distribution with the system. As the Weissenberg number gets higher, the surface of the fluid gets hotter and the thickness of the thermal boundary layer increases.

Figures 12 and 13 show how the temperature of the fluid is affected by parameters (α and β) that control heat absorption and generation. When α is a positive number and β is a positive number, it means that heat is being produced inside. When α is a negative number and β is a negative number, it means that heat is being absorbed from the inside. The combined impact of the heat source/sink factors decides how much the temperature changes in the boundary layer region. Also, the layer of heat around the heat source is larger than the layer of heat around the heat sink. We are looking at the impact of ω (thermal slip parameter) using Figure 14 to help us understand it. Increasing values of ω cause the fluid temperature, θ(η), to go down. This happens because it makes less heat and cools down the fluid.

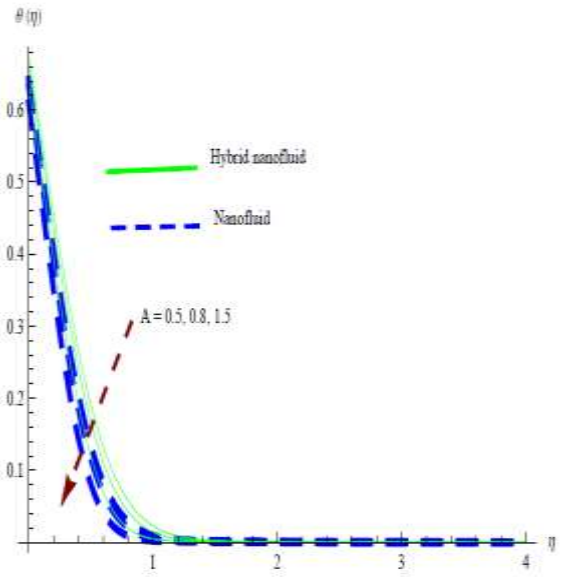

Figure 9: Impact of wedge's stretching parameter of fluid's temperature

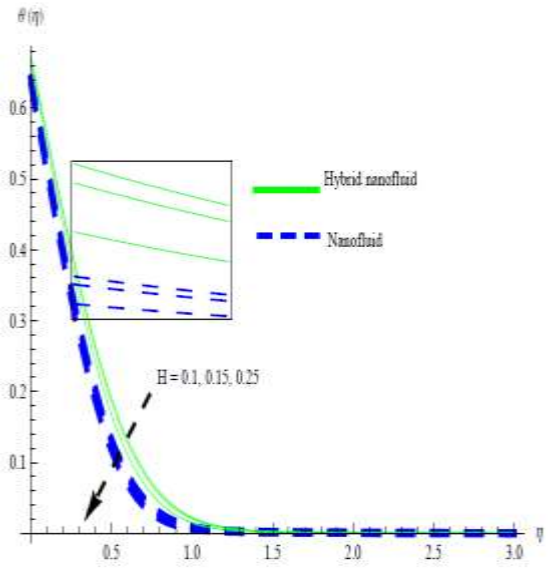

Figure 10: Influence of magnetic field on induced magnetic field profile

*Corresponding author, e-mail: peteroolmi@yahoo.com
DIO

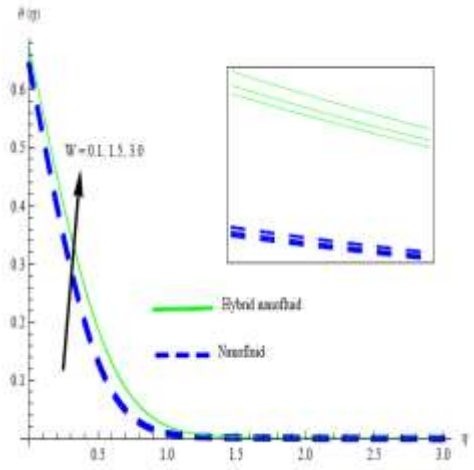

Figure 11: Effect of Weissenberg number on temperature profile

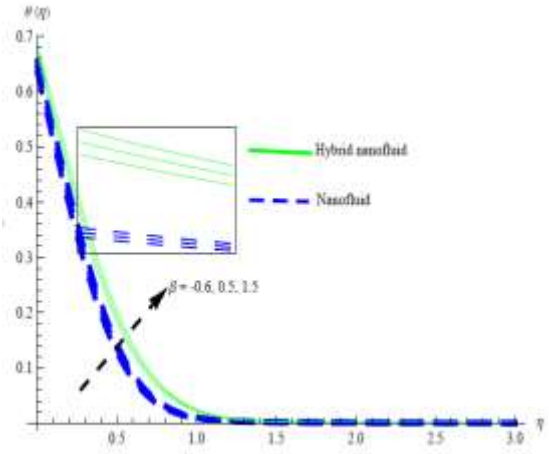

Figure 12: Impact of heat absorption/generation on temperature profile

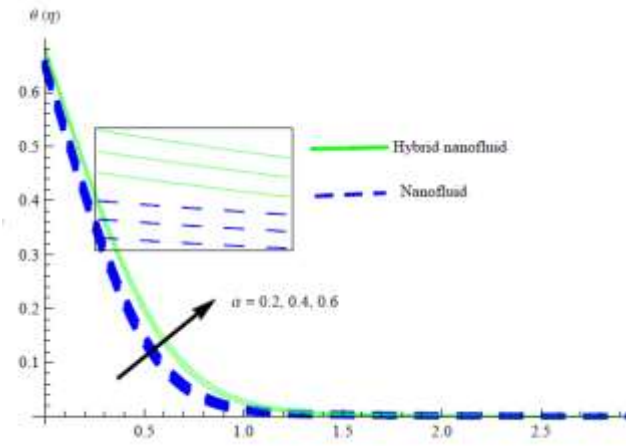

Figure 13: Variation of heat absorption/generation on temperature profile

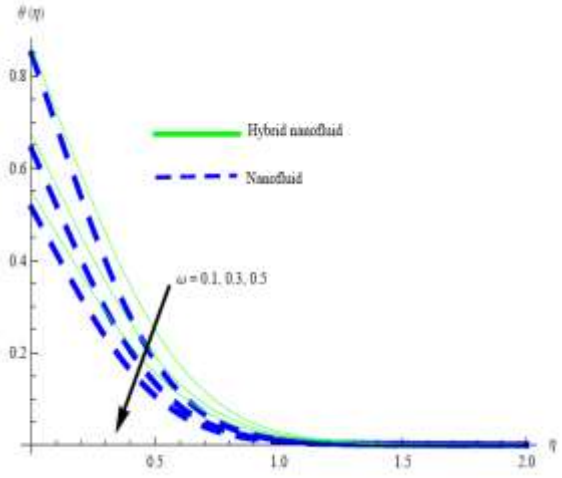

Figure 14: Influence of thermal slip parameter on temperature profile

4. CONCLUSION

The influences of Slip and induced magnetic field on tangential hyperbolic hybrid nano-fluid over a stretching wedge with non-uniform heat source are examined using homotopy analysis method. The summary of the findings on the flow and heat characteristics are:

- An increase in the stretching parameter (A) of the wedge and magnetic field parameter (H) had a comparable effect on the hybrid nanofluid's fluid motion, whereas the opposing effect is observed for non-Newtonian Weissenberg number (W).
- The induced magnetic field improved by increasing magnetic field parameter and reciprocal of induced prandtl number parameter (λ), but decreases by escalating the stretching parameter and the Weissenberg number.

- The thermal distribution enhanced significantly with the rise in thermal slip parameter, and heat absorption/generation parameters but declines with the rise in the stretching parameter, Weissenberg number, and magnetic field parameter.
- Skin friction coefficient is enhanced by escalating the stretching parameter, magnetic field parameter and reciprocal of induced prandtl number parameter.
- The Nusselt number grows with variation in thermal slip parameter, radiation parameter (Rd), heat absorption/generation parameters but reduces with change in the stretching parameter, magnetic field parameter and reciprocal of induced prandtl number parameter for both fluids.
- Solutions obtained using HAM agreed greatly with published data, demonstrating the effectiveness and dependability of the method.

Reference

Afify, A. A. Uddin, M. J. & Ferdows, M., (2014). "Scaling group transformation for MHD boundary layer fow over permeable stretching sheet in presence of slip flow with Newtonian heating efects," Applied Mathematics and Mechanics-English Edition, 35 (11), 1375–1386.

Akindele M Okedoye, Azeez A Waheed, & Peter O Ogunniyi (2022) Effect of Convective Surface Boundary Condition MHD Heat and Mass Transfer over a Vertical Plate with Buoyancy and Chemical Reaction. Journal of Engineering and Applied Sciences Technology. SRC/JEAST-184. DOI: doi.org/10.47363/JEAST/2022(4)147

Ali, F. M., Nazar, R., Arifin, N. M. & Pop, I., (2011). MHD boundary layer flow and heat transfer over a stretching sheet with induced magnetic field, Heat Mass Transf. 47, 155–162, https://doi.org/10.1007/s00231-010-0693-4.

Alphonsa, M., Sujesh, A., Sabu, A. S. & Saleem, S., (2021) Significance of multiple slip and nanoparticle shape on stagnation point flow of silver-blood nanofluid in the presence of induced magnetic field. Surfaces and Interfaces 25:101267 [https://doi.org/10.1016/j.surfn.2021.101267]

Aziz, A., Siddique, J. I., & Aziz, T. (2014). Steady Boundary Layer Slip Flow along with Heat and Mass Transfer over a Flat Porous Plate Embedded in a Porous Medium. *PLOS ONE*, *9*(12), e114544. https://doi.org/10.1371/journal.pone.0114544

Beavers, G. S. & Joseph, D. D., (1967). "Boundary conditions at a numerically permeable wall," Journal of Mechanics, 0, 197–207

Bidin B, & Nazar R., (2009). Numerical solution of the boundary layer flow over an exponentially stretching sheet with thermal radiation. Eur J Sci Res 33(4):710–717.

Carragher P, & Crane LJ., (1982). Heat transfer on a continuous stretching sheet. ZAMM Z Angew Math Mech 62, 564–73.

Crane LJ. Flow past a stretching plate. Z Angew Math Phys 1970;21: 645–55.

Gbadeyan, J. A., Abubakar, J. U., & Oyekunle, T. L., (2020). Effects of Navier slip on a steady flow of an incompressible viscous fluid confined within spirally enhanced

channel. Journal of the Egyptian Mathematical Society 28(1), DOI: 10.1186/s42787-020-00081-9

Hayat, T., Farooq, M., & Alsaedi, A., (2015). Homogeneous-heterogeneous reactions in the stagnation point flow of carbon nanotubes with Newtonian heating, AIP Adv 5, 27130, https://doi.org/10.1063/1.4908602.

Hayat, T., Muhammad, K., Farooq, M., & Alsaedi, A., (2016). Melting heat transfer in stagnation point flow of carbon nanotubes towards variable thickness surface, AIP Adv 6, 15214, https://doi.org/10.1063/1.4940932.

Ishak A., (2011). MHD boundary layer flow due to an exponentially stretching sheet with radiation effect. Sains Malays 40:391–5.

Ishak, A., Nazar, R., & Pop, I., (2006). Mixed convection boundary layers in the stagnation-point flow toward a stretching vertical sheet, *Meccanica*, 41(5),509–518, 2006.

Kumari, M., Takhar, H. S. & Nath, G., (1990). MHD flow and heat transfer over a stretching surface with prescribed wall temperature or heat flux, Warme ¨ - Und Stoffübertragung 25, 331–336, https://doi.org/10.1007/BF01811556.

Liao S.J., (1992). The proposed homotopy analysis technique for the solution of non-linear problems (Ph.D. thesis), Shanghai Jiao Tong university.

Liao, S.J., & Campo, A., (2002). Analytic solutions of the temperature distribution in Blasius viscous flow problems. Journal of Fluid Mechanics, 453 -425.

Mabood, F, Yusuf, T.A., & Khan, W.A., (2020). Cu-Al_2O_3-H_2O hybrid nanofluid flow with melting heat transfer, irreversibility analysis and nonlinear thermal radiation. Journal of Thermal Analysis and Calorimetry, published online: 10.1007/s10973-020-09720-w.

Magyari E, & Keller B., (1999). Heat and mass transfer in the boundary layers on an exponentially stretching continuous surface. J Phys D: Appl Phys 32:577–85.

Mahapatra, T. R. & Gupta, A. S., (2002). "Heat transfer in stagnation point flow towards a stretching sheet," *Heat and Mass Transfer*, 38(6), 517–521.

Mohamed A. El-Aziz & Ahmed A., (2018). Afify. Influences of Slip Velocity and Induced Magnetic Field on MHD Stagnation-Point Flow and Heat Transfer of Casson Fluid over a Stretching Sheet Mathematical Problems in Engineering. Article ID 9402836, 1-11 https://doi.org/10.1155/2018/9402836

Ogunniyi, P.O.**,** Gbadeyan, A.J., Agarana, M.C., & Yusuf, T.A. (2022) Nonlinear thermal radiation on MHD tangential hyperbolic hybrid nanofluid over a stretching wedge with convective boundary condition, Heat Transfer, **51**(6), 5417–5440.

Partha MK, Murthy PVSN & Rajasekhar GP, (2005). Effect of viscous dissipation on the mixed convection heat transfer from an exponentially stretching surface. Heat Mass Transfer 41:360–6.

Waini, I., ishak, A., & Pop, I., (2020). MHD flow and heat transfer of a hybrid nanofluid past a permeable stretching/shrinking wedge. Applied Mathematics and Mechanics

(English Edition), 41(3), 507–520
https://doi.org/10.1007/s10483-020-2584-7